Low Temperature Physics/Fizika Nizkikh Temperatur, 2018, v. 44, No. 5, pp. 561–567

Features of spin dynamics in HgCrCdSe and HgCrSe crystals in the vicinity of phase transitions

B.E. Bekirov, I.V. Ivanchenko, and N.A. Popenko

O.Ya. Usikov Institute for Radiophysics and Electronics of the National Academy of Sciences of Ukraine
12 Ac. Proskura str., Kharkov 61085, Ukraine
E-mail: ireburan@yahoo.com

Received September 29, 2017, revised December 5, 2017, published online March 27, 2018

The inhomogeneously broadened EPR lines of the solid solutions $Hg_{1-x-y}Cr_xCd_ySe$ and $Hg_{1-x}Cr_xSe$ are represented in the form of spin packets and their temperature evolution is analyzed upon the transition of the crystals to ferromagnetic ordering. In this case, the spin packets being introduced into the consideration are identified with allowed transitions of the localized electrons and with the delocalized electrons. It is established that a characteristic feature of the subsystem of delocalized electrons is the anomalous behavior of the *g*-factor in the vicinity of the transition to the ferromagnetic state. The introduced spin subsystems, which characterize the localized and delocalized electronic states, allow for explainig the differences in scenarios of the transition to magnetic ordering of crystals with different cluster structures. Just significantly lower concentration of clusters in the HgCrSe crystal leads to a slowing down of flip-flop processes that explains the longer relaxation times of spin packets in this diluted magnetic semiconductor in comparison with the relaxation times of spin packets in the HgCrCdSe crystal in the ferromagnetic temperature range.

PACS: 76.30.–v Electron spin resonance and relaxation;
76.30.Da Ions and impurities: basic;
75.50.Pp Magnetic semiconductors.

Keywords: electron paramagnetic resonance, spin packet, relaxation.

1. Introduction

Taking into account that the diluted magnetic semiconductor (DMS) are classified as a class of magneto-diluted spin systems with the dipole interaction due to the randomness of the spatial distribution of the spins on a crystal lattice, the speed of their “flip-flops” is much slower than the speed of transverse (or spin-spin) relaxation of spins [1,2]. Therefore the inhomogeneous broadening of the absorption lines is typical for the EPR spectra of such systems.

It is known that the description of absorption lines like that is based on the concept of Portis [3] on the representation of such lines in the form of a set of equivalent paramagnetic centers (“spin packets”) with the same Larmor frequencies and different *g*-factors, when each spin packet separates a part of the inhomogeneously broadened ESR line, which behaves homogeneously with respect to external influences, such as a lattice or the electromagnetic radiation. This approach has been proven to be used in the theory and practice of magnetic resonance spectroscopy by other authors [1,4–6].

In our research we apply the aforementioned concept for the description of the experimental EPR spectra and use the term “spin packet” as an individual line describing the absorption signal from the set of spins with the same Larmor frequency, without imposing additional conditions on the infinite number of packets of the same physical origin with a continuous spectral distribution. From our point of view, this approach is expedient and promising for the analysis of physical processes in DMS (in particular, in the solid solutions $Hg_{1-x}Cr_xSe$ and $Hg_{1-x-y}Cr_xCd_ySe$) in which a paramagnetic response is produced by both the localized and delocalized electrons [7]. In doing so, we take into account the fact that the difference in the *g*-factors of spin packets can be due to the different position of the paramagnetic center in the coordination complex of these crystals [8]. Furthermore, the possible difference in the concentration of paramagnetic centers in the spin packets can lead to different widths and integrated line intensities.

Then, under conditions of the weak SHF power, when the balance in the spin system is not disturbed, the knowledge of the temperature evolution of spin packet

parameters can be very useful, in particular, for analyzing the behavior of allowed transitions in the magnetically diluted systems, especially in the vicinity of phase transitions. In this paper, we use this approach to studying the magnetoresonance properties of two aforementioned DMS with the concentration of a paramagnetic impurity that does not lead to splitting of the EPR line with the temperature decrease [7].

It was found earlier [8,9], that in both types of crystals the transition to a ferromagnetic ordering phase occurs as a result of *s–d* exchange interaction on the RKKY mechanism [10]. The studies of magnetic moments were carried out on the SQUID magnetometer MPMS-XL5 device. The measured dependences point out the transition of the solid solution $Hg_{0.5}Cd_{0.4}Cr_{0.1}Se$ to the ferromagnetic ordered phase occurs at the Curie temperature T_C = (126 ± 1) K [9] while the transition of the solid solution $Hg_{0.97}Cr_{0.03}Se$ to the ferromagnetic ordered phase occurs at T_C = (106 ± 1) K that is inherent to the $HgCr_2Se_4$ ferromagnetic spinel [11].

The main purpose of this research is studying the temperature evolution of spin packets to reveal the features and differences of the spin dynamics in the HgCrCdSe and HgCrSe crystals at the transition of these DMS to the ferromagnetic ordering.

2. Samples and methods

In this research we focus on the investigations of EPR spectra of the solid solutions $Hg_{0.97}Cr_{0.03}Se$ and $Hg_{0.5}Cd_{0.4}Cr_{0.1}Se$ grown in the Chernivtsi National University by the solid state recrystallization method, which in contrast to the Bridgman's method allows obtaining a more homogeneous distribution of the Hg, Cr, and Se components.

The microanalysis of the samples was performed on the scanning electron microscope ZEISS EVO 50XVP with a combined system of the energy-dispersion analysis INCA ENERGY 450 and structural HKL Channel 5 analysis. We used the operational mode of the spectrometer so that the analyzed surface area of the sample was less than 1 μm. The Fig. 1 illustrates the typical electronic images of the surface fragments of the samples [8,9].

The analysis of the percentage content of elements has shown that the dark areas on the electron-diffraction pattern of the HgCrSe sample correspond to the spinel phase $HgCr_2Se_4$ [8] (Fig. 1(a)). At the same time the dark areas on the electron-diffraction pattern of the HgCdCrSe sample correspond to the four-component compound HgCdCrSe while the light areas correspond to the nonmagnetic three-component compound HgCdSe [9] (Fig. 1(b)). This gives us reason to believe that just the presence of a four-component compound HgCdCrSe in the nonmagnetic matrix HgCdSe will determine the magnetic and magnetoresonance properties of these samples.

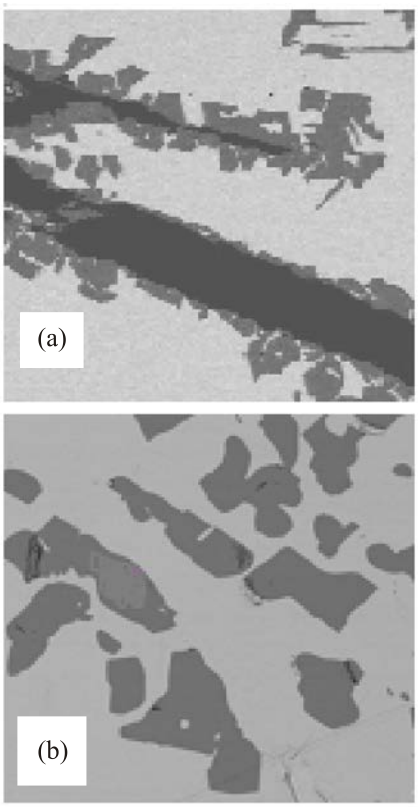

Fig. 1. Electron-diffraction patterns of the HgCrSe (a) and HgCdCrSe (b) crystals.

Thus, two different compounds coexist in each of the samples under test. It is worth noting that the chromium content in such a four-component compound in percentage (18.96%) is higher, than that in the spinel clusters $HgCr_2Se_4$ (14%).

Thus, in the samples under test, an inhomogeneous structure is formed during their growth, which consists of both the nonmagnetic and magnetic phases. In the three-component solid solution $Hg_{1-x}Cr_xSe$ two types of paramagnetic inclusions are present, and two coordination complexes such as tetrahedral (HgCrSe) and octohedral ($HgCr_2Se_4$) are considered in accordance with [8]. At the same time, in the four-component solid solution $Hg_{1-x-y}Cr_xCd_ySe$ only one type of paramagnetic inclusions such as HgCdCrSe occurs and, consequently, a one tetrahedral coordination complex is considered.

The EPR spectra were measured on the *X*-band superheterodyne spectrometer operating in the temperature range 1.7–300 K. The sensitivity of the spectrometer is $5 \cdot 10^{14}$ spins/T. The accuracy of measuring the external magnetic field is $\pm 10^{-4}$ T in the range 0–0.7 T that makes it possible to determine the *g*-factor with an accuracy of $\pm 1 \cdot 10^{-3}$. Spectrometer assures the accuracy of the measurement and stabilization of the temperature ±0.01 and ± 0.1 K, respectively.

3. Electron spectra of Cr^{3+} ion

It was shown in [8] that the EPR signal observed in experiments at temperatures above the nitrogen ones is originated by the Cr^{3+} ion. The calculations of the electron spectrum for the high-spin state of the Cr^{3+} ion located in both the cubic and tetrahedral environments have shown that in the undistorted octahedral complex $(CrSe_6)^{9-}$ and tetrahedral complex $(CrSe_4)^{5-}$, the chromium ion is to be trivalent and has an electron configuration of the valence shell with the main term ^4F. The crystal field splits this basic electron term of the Cr^{3+} ion into the three crystal terms depending on the ligand's symmetry: in the case of tetrahedral symmetry $^4F = {}^4A_1 + {}^4T_2 + {}^4T_1$, while in the case of cubic symmetry $^4F = {}^4A_{2g} + {}^4T_{2g} + {}^4T_{1g}$. In this case, the orbital triplet $^4T_1$ in the tetrahedral case and the orbital singlet $^4A_{2g}$ in the cubic case are the basic ones [12]. Spin-orbit coupling does not result in the evident splitting of the $^4A_{2g}$ term while the crystal triplet $^4T_2$ splits into the two spin quartets and two spin doublets in such a way that one of the spin quartets is the lowest level. Thus, in both the undistorted tetrahedral and octahedral crystal fields the spin quartet is the ground state. An external magnetic field splits the aforementioned spin quartets in a different way (Fig. 2).

In the case of the octahedral crystal field, the arbitrarily directed magnetic field splits the lowest $^4A_{2g}$ quartet into the four spin singlets, which are equidistant, and the transitions 1↔2, 2↔3 and 3↔4 are to be the allowed transitions (Fig. 2(a)).

In the tetrahedral case, the lowest quartet splits into the two quasi-doublets in such a way that the splitting between quasi-doublets is much bigger than those located inside the quasi-doublets. The transition 1↔2 has vanishingly small intensity, i.e., it is forbidden, whereas the transitions 1↔3 and 1↔4 as well as 2↔3 and 2↔4 are to be the allowed transitions (Fig. 2(b)). Thus, the EPR signal originates from the transitions between two quasi-doublets and the 1↔4 transition is considered as the main representative [8].

4. Research results

Spin-packet concept we applied to the experimental EPR spectra of HgCrSe and HgCdCrSe crystals published in our previous papers [8,9].

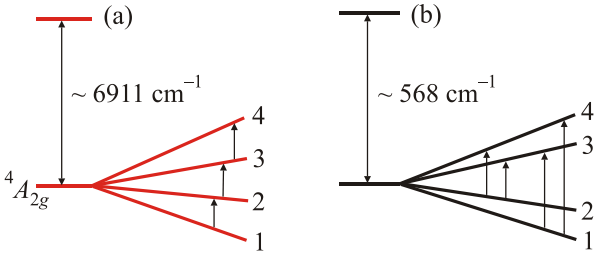

Fig. 2. The schemes of the Cr^{3+} ion level-splitting in the case of octahedral (a) and tetrahedral (b) crystal fields.

When the EPR line was approximated, the resonance position and the width of spin packets, as well as their number and intensity varied. Calculations were carried out for both the Lorentzian and the Gaussian forms of the spin packet. As it follows from the results of investigations, the experimental spectra for both crystals are good approximated by the ten spin packets of the Gaussian shape. But only the first four spin packets have the intensity exceeding the limits of the confidence intervals of the detected EPR signals. These spin packets are located non-equidistantly, have different Larmour frequencies, widths and integral intensity because they are located in different conditions. The intensities of remaining spin packets are negligible and are within the confines interval of the detected EPR signal.

Taking into account a sensitivity of the radio spectrometer used, we limited ourselves to the ratio of the levels of the noise track and the detected EPR signal to no more than 2%. As the result, the determination coefficients were as follows: 0.9957 (T = 215 K) and 0.9894 (T = 87 K) for the HgCdCrSe crystal; 0.9955 (T = 207 K) and 0.9877 (T = 85 K) for the HgCrSe crystal.

The examples of such approximation for two characteristic temperatures, namely before and after the transition to the ferromagnetic phase, show a good agreement with the experimental data (Fig. 3).

A characteristic feature of DMS with an unfilled 3*d*-shell, to which the solid solutions $Hg_{1-x}Cr_xSe$ and $Hg_{1-x-y}Cr_xCd_ySe$ are related, is that they contain along with the conduction electrons (delocalized spins) and 3*d*-electrons localized on the appropriate atoms. To describe the kinetics of the processes in such systems, the localized and delocalized spins (which are the mediators between the paramagnetic centers in the RKKY mechanism) are represented in the form of two subsystems "*d*" and "*s*", in which the interaction between them occurs with the appropriate rates V_{ds} and V_{sd} [13].

5. HgCrSe crystals

Following the temperature dependences of spin packet parameters (Fig. 4) it can be stated that in the temperature interval ranging from the room temperature to T = 128 K the *g*-factor of spin packets remains virtually unchanged. In the temperature range T = 128–110 K, foregoing to the transition of the spinel to the ferromagnetic state (we call it the transition region), their absolute values undergo different changes, namely: for two spin packets described by curves *1* and *2*, the *g*-factors begin increase, while for the other two spin packets the *g*-factors begin decrease with some anomaly in the behavior of the *g*-factor, described by the curve *3*, near the temperature $T \approx 120$ K. After the transition of spinel clusters to the ferromagnetic ordering (T < 106 K), the *g*-factors of the first pair of spin packets (curves *1* and *2*) continue to increase, reaching the values

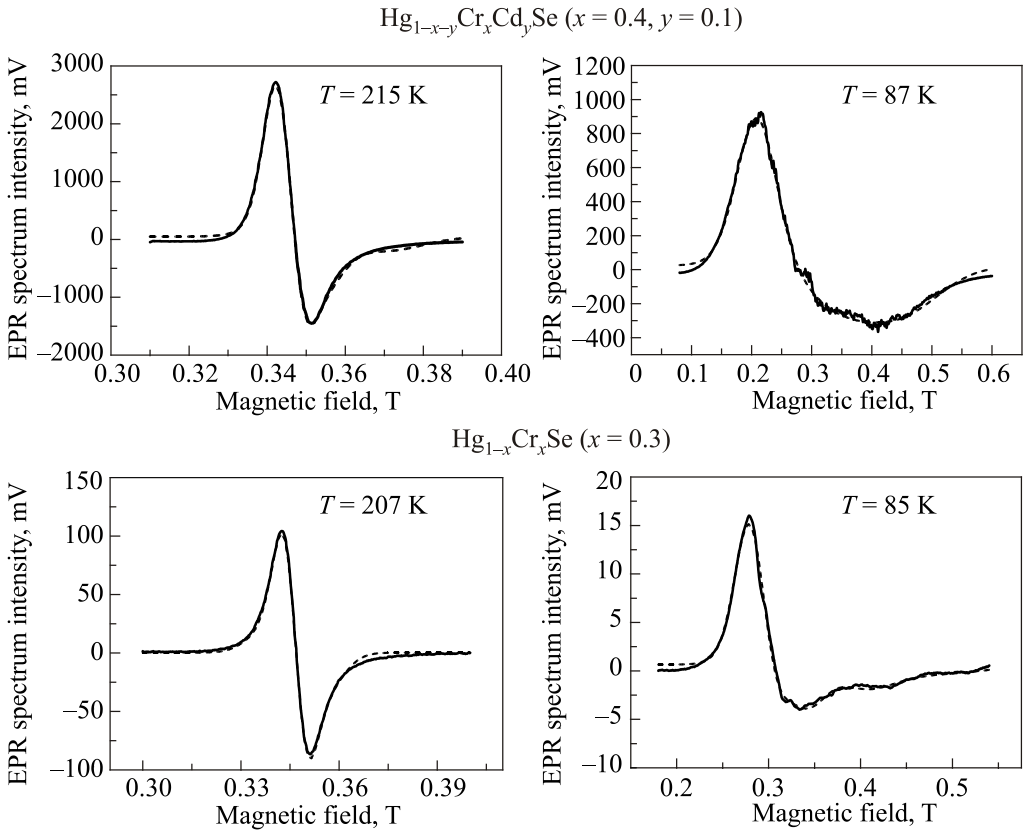

Fig. 3. EPR spectra of HgCdCrSe and HgCrSe crystals: experiment (solid line), approximation (dotted line).

2.5 and 2.9 at T = 85 K, while the g-factors of the second pair of spin packets (curves *3* and *4*) tend to the value $g \approx 1.8$.

The revealed behavior of the g-factors of spin packets (Fig. 4(a)) can be explained by introducing the following conventional classification, namely: in the subsystem "*d*" of localized electrons the spin packets described by the curves *1*, *2* and *4* may refer to the allowed transitions 1↔2, 2↔3 and 3↔4 in accordance with a scheme of the Cr^{3+} ion level-splitting in the octahedral crystal field (see Fig. 2(a)), while the spin packet described by the curve *3* refers to the subsystem "*s*" of delocalized electrons. In accordance with [8], in this case the trigonal perturbations of the crystal field are the most probable ones and the development of those with the temperature decrese results in the decrease of the octahedron cell volume and, hence, in an increase of the crystal field strength that may be the reason for the difference in the temperature dependences of the g-factors of spin packets of the subsystem "*d*" of localized electrons.

The widths of spin packets from the room temperature to T = 128 K vary slightly (Fig. 4(b)) and begin to broaden noticeably in the transition region in accordance with the increase in the EPR line width when the temperature decreases, that is characteristic for the mixed-valence spinel ferrites during the establishment of magnetic ordering in the system [14]. In this case, the anomalous change in the width of the spin packet at the temperature $T \approx 120$ K (as well as the g-factor described by the curve *3* in the Fig. 4(a) confirms the legitimacy of the aforementioned classification of spin packets, since in the vicinity of $T \approx 120$ K a sharp change in the conductivity of the $HgCr_2Se_4$ crystal occurs [15]. After the phase transition, the widths of spin packets, described by the curves *2*, *3*, *4*, increase sharply, while the curve *1* slows down its growth.

With the temperature decrease, the integrated intensities of spin packets described by the curves *1*, *2* and *4* increase monotonically, reaching the maximum values in the region of the phase transition of the spinel to the ferromagnetic state and decrease below the Curie point ($T < T_C$ = 106 K) (Fig. 4(c)). At the same time, the integral intensity of the spin packet described by the curve *3* increases monotonically throughout the analyzed temperature range.

The values of T_2 were determined from the well-known equation for the single symmetric lines [16], which are the spin packets obtained as a result of the approximation:

$$T_2 = 1.3131 \cdot 10^{-7} / g \Delta H_{pp}^0,$$

where the values of the g-factor and the width ΔH of a single symmetric line included in this equation were taken for each spin packet and the values of T_2 were calculated for each temperature.

As follows from the Fig. 4(d), when the sample is cooled, the spin-spin relaxation times T_2 of spin packets decrease

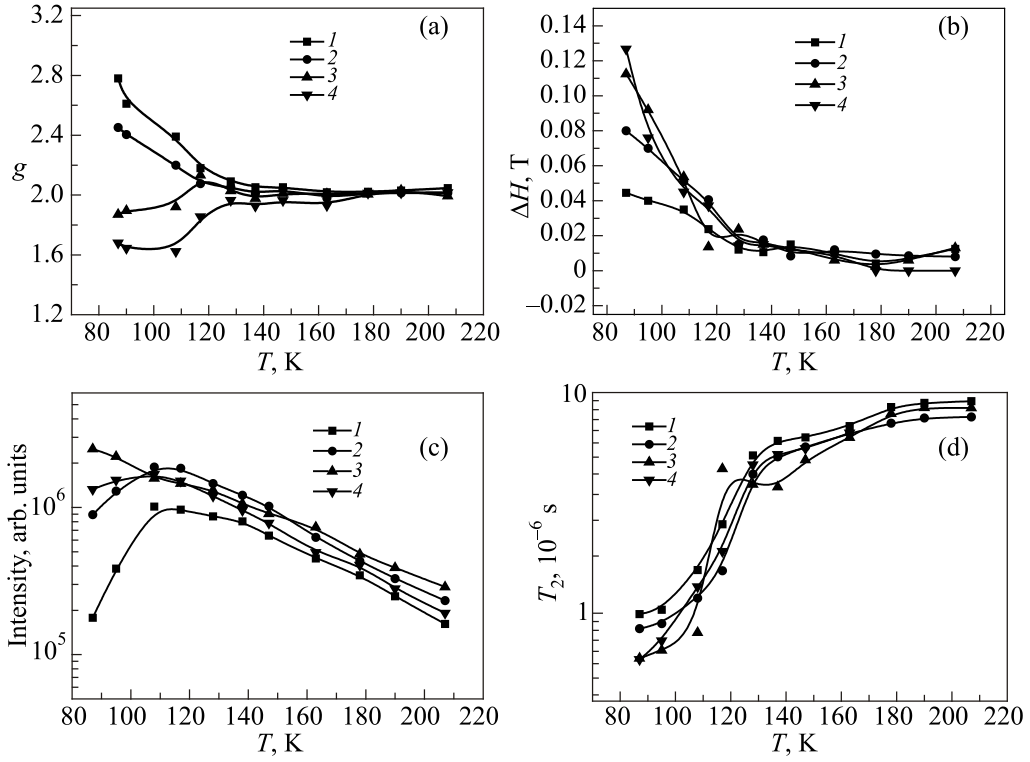

Fig. 4. Temperature dependences of *g* factor (a), width (b), integral intensity (c) and spin-spin relaxation time (d) of the spin packets that approximate the EPR lines of the solid solution $Hg_{0.97}Cr_{0.03}Se$ (the numbers *1–4* denote belonging to the appropriate spin packets).

monotonically by a factor of 2 from $T_2 \approx (8–9)\cdot10^{-6}$ s at $T = 207$ K to $T_2 \approx (4–5)\cdot10^{-6}$ s at $T \approx 128$ K. In the transition region ($T = 128–110$ K), the relaxation times decrease by more than 3 times, taking the values $T_2 \approx (1.2–1.6)\cdot10^{-6}$ s, excepting the anomaly near the temperature $T = 120$ K for the spin packet described by the curve *3*. And after the transition of the ferromagnetic spinel $HgCr_2Se_4$ to the ferromagnetic state ($T < 100$ K), the relaxation times of two spin packets (curves *1* and *2*) referring to the subsystem "*d*" tend to the values $T_2 \approx 9\cdot10^{-7}$ s and $8\cdot10^{-7}$ s, while the relaxation times of third spin packet of the subsystem "*d*" (curve *4*) and the spin packet referring to the subsystem "*d*" of delocalized electrons (curve *3*) become equal ($V_{ds} \approx V_{sd}$).

6. HgCdCrSe crystals

As it shown by the results of microanalysis (see Fig. 1(b)) the solid solution $Hg_{0.5}Cd_{0.4}Cr_{0.1}Se$ has a cluster structure with the chaotic distribution of clasters in the bulk of the DMS. Namely, in the nonmagnetic matrix formed by the three-component compound HgCdSe, there are the clusters HgCdCrSe with the magnetically active chromium ions, which determine the magnetic and magnetoresonance properties of these crystals. It should be noted that the chromium content in HgCdCrSe compounds is higher than that in clusters of ferromagnetic spinel $HgCr_2Se_4$ in the solid solution $Hg_{0.97}Cr_{0.03}Se$ [9]. The substitution of Cr^{3+} ions in the host tetrahedral matrix (see Fig. 2(b)) provides the additional degree of freedom for the off-centered shifting of the chromium ion as well as for the distortion of the ligand's cell, which can increases with the temperature decrease.

As can be seen from the Fig. 5(a), the *g*-factors of spin packets (as in the case of HgCdSe) remain virtually unchanged in the temperature interval ranging from the room temperature to $T = 157$ K. In the transition region ($126 \text{ K} < T < 160$ K), for the two spin packets described by the curves *1* and *2*, the *g*-factors increase slightly and sharply increase after the crystal transition to the ferromagnetic ordering, reaching the values 2.9 and 2.72 at $T = 87$ K. It is quite clear that with the temperature decrease the chromium off-centering shift increases resulting in the increase of the *g*-factor. Here, on the temperature dependences of *g*-factors of two other spin packets described by the curves *3* and *4* one can see the maxima in the vicinity of the phase-transition temperature ($T \approx 126$ K). At the temperature $T = 87$ K the *g*-factors are 1.92 and 1.87, respectively. The aforementioned dependences of *g*-factors allow one to introduce the following classification of spin packets, namely: in accordance with a scheme of the Cr^{3+} ion level-splitting in the tetrahedral crystal field (see Fig. 2(b)) in the subsystem "*d*" of localized electrons, the spin packets described by the curves *1* and *2* may refer to the allowed transitions $1\leftrightarrow4$ and $1\leftrightarrow3$ as the main representative [8], while the spin packets described by the curves *3* and *4* can be attributed to the subsystem "*s*" of delocalized electrons.

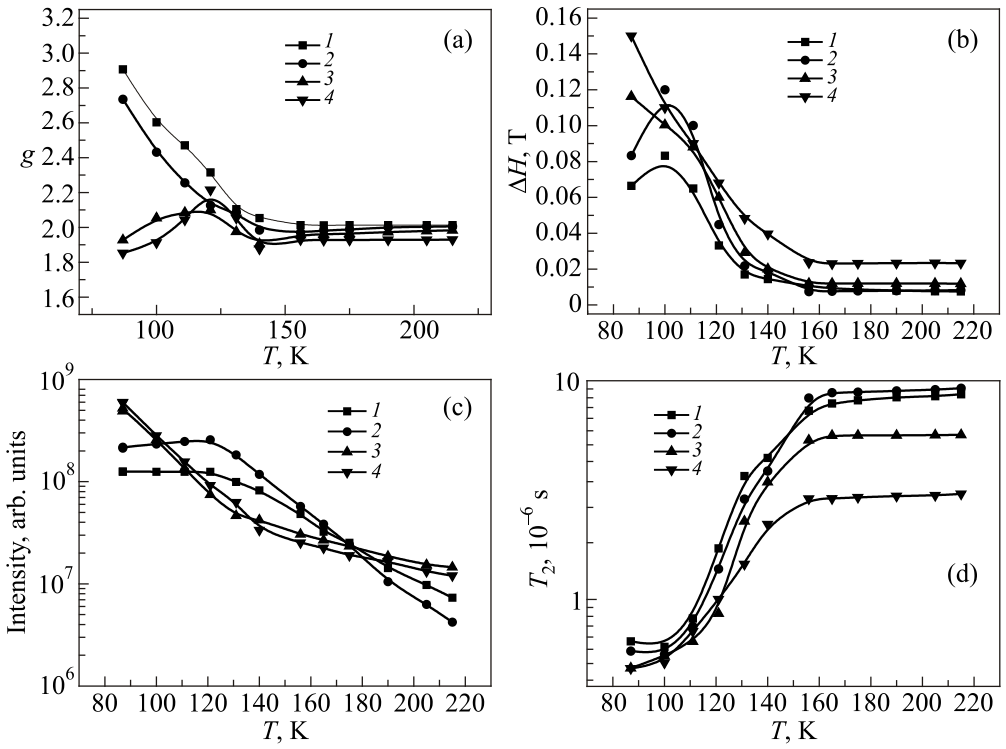

Fig. 5. Temperature dependences of *g* factor (a), width (b), integral intensities (c) and spin-spin relaxation time (d) of the spin packets that approximate the EPR lines of the solid solution $Hg_{0.5}Cd_{0.4}Cr_{0.1}Se$ (the numbers *1–4* denote belonging to the appropriate spin packets).

As for the widths of the spin packets, they remain virtually unchanged in the temperature interval ranging from the room temperature to T = 157 K (Fig. 5(b)). In the transition region the packets begin to broaden. After the crystal transition to ferromagnetic ordering (T < 126 K), the widths of two spin packets continue to increase (curves *3* and *4*), while the widths of other two spin packets (curves *1* and *2*) start to decrease, illustrating the characteristic extreme dependence and indicating a change in the dominating mechanisms of the spin interaction after the phase transition, namely, pointing out the increase of the exchange interaction on the RKKY mechanism.

With the temperature decrease, the integrated intensities of spin packets described by the curves *1* and *2* increase monotonically, reaching the maximum values in the region of the phase transition, and do not undergo any visible changes below the Curie point ($T < T_C$ = 126 K) (Fig. 5(c)). At the same time, the integrated intensities of spin packets described by the curves *3* and *4* increase throughout the analyzed temperature range, as in the case of the curve *3* in HgCrSe (see Fig. 4(c)).

As it follows from the Fig. 5(d), when the temperature decreases (from the room temperatures to $T \approx 157$ K), the transverse relaxation times T_2 of all spin packets remain virtually unchanged, but they have some different absolute values. For the spin packets of the subsystem "*d*" of localized electrons (curves *1* and *2*) referring to the allowed transitions 1↔4 and 1↔3 (Fig. 2(b)), the time $T_2 \approx 9\cdot10^{-6}$ s, while for the spin packets of the subsystem "*s*" of delocalized electrons (curves *3* and *4*), these times are equal to $T_2 \approx 5.5\cdot10^{-6}$ s and $T_2 \approx 3\cdot10^{-6}$ s, respectively. Beginning with T = 157 K and lower, the relaxation times of all spin packets decrease sharply up to $T \approx 110$ K, taking the values $T_2 \approx (6.5–8.0)\cdot10^{-7}$ s. At T < 100 K the relaxation times of spin packets (curves *1* and *2*) referring to the subsystem "*d*" of the localized electrons tend to the value $T_2 \approx 6\cdot10^{-7}$ s while the relaxation times of spin packets (curves *3* and *4*) referring to the subsystem "*s*" of delocalized electrons become equal $T_2 \approx 4.8\cdot10^{-7}$ s. It should be noted that the error in determining the spin-spin relaxation times does not exceed $2\cdot10^{-8}$ s.

7. Conclusions

For the first time the concept of spin packets for the description of inhomogeneously broadened EPR lines with respect to the DMS has been applied. It is shown that the inhomogeneously broadened EPR lines of the solid solutions $Hg_{1-x-y}Cr_xCd_ySe$ and $Hg_{1-x}Cr_xSe$ are well approximated by the four spin packets. The analysis of temperature dependences of the *g*-factors of spin packets and the comparison of the obtained data with the results of calculations of the electron spectra of the Cr^{3+} ion located in the cubic ($HgCr_2Se_4$) and tetrahedral (HgCrSe and HgCdCrSe) environment [8] pointed out that for the HgCrSe crystal three spin-packets can be correlated with the allowed tran-

sitions in the subsystem "*d*" of localized electrons and a one spin-packet — with the subsystem "*s*" of delocalized electrons. Unlike the HgCrSe crystal, in the HgCdCrSe crystal two spin-packets refer to the allowed transitions in the subsystem "*d*" of localized electrons and two spin-packets — to the subsystem "*s*" of delocalized electrons.

The features of spin dynamics in HgCrCdSe and HgCrSe crystals in the vicinity of phase transitions have been revealed, namely: (i) the temperature interval of the transition of the HgCrCdSe crystal exceeds twice that of the HgCrSe crystal; (ii) unlike the HgCrSe crystal the difference in the *g*-factors, widths, and spin-spin relaxation times of both spin packets related to the delocalized electrons of the HgCrCdSe crystal are diminished at $T < 100$ K; (iii) in the ferromagnetic temperature region the relaxation times of spin packets for the HgCrSe crystal (subsystem "*d*"↔$T_2 \approx 9\cdot10^{-7}$ s and $8\cdot10^{-7}$ s; subsystem "*s*"↔ $T_2 \approx \approx 6\cdot10^{-7}$ s) are longer than for the HgCrCdSe crystal (subsystem "*d*"↔$T_2 \approx 6\cdot10^{-7}$ s; subsystem "*s*"↔$T_2 \approx 4.8\cdot10^{-7}$ s); (iv) unlike the HgCdCrSe crystal, the presence of two different phase states in the HgCrSe crystal (HgCrSe and $HgCr_2Se_4$) leads to the flip-flop slowing.

1. V.A. Atsarkin, G.A. Vasneva, and V.V. Demidov, *Sov. Phys. JETP* **64** (4), 898 (1986).
2. V.A. Atsarkin, V.V. Demidov, and G.A. Vasneva, *Phys. Rev. B* **56** (15), 9448 (1997).
3. A.M. Portis, *Phys. Rev*. **91**, 1071 (1953).
4. G. Castner, *Phys. Rev*. **115**, 1506 (1959).
5. L.L. Buishvilli, M.D. Zviadadze, and G.R. Khutsishvili, *Zh. Eksp. Teor. Fiz.* **56**, 290 (1969) [*Sov. Phys. JETP* **29**, 159 (1969)].
6. V.A. Azarkin, *Dynamic Polarization of Nuclei in Solid Lielectrics*, Nauka, Moscow (1980) (in Russian).
7. K.W. Edmonds, P. Bogusławski, K.Y. Wang, R.P. Campion, and S.N. Novikov, *Phys. Rev. Lett.* **92**, 037201 (2004).
8. K. Lamonova, I. Ivanchenko, S. Orel, S. Paranchich, V. Tkach, E. Zhitlukhina, N. Popenko, and Yu. Pashkevich, *J. Phys.: Condens. Matter* 21 (4), 045603 (2009).
9. B. Bekirov, I. Ivanchenko, N. Popenko, A. Bludov, V. Pashchenko, and V. Tkach, *Appl. Magn. Reson*. **45** (1), 75 (2014).
10. G.S. Krinchik, *Physics of Magnetic Phenomena*, Moscow University (1976) (in Russian).
11. P.K. Baltzer, P.J. Wojtovicz, M. Robbins, and E. Lopatin, *Phys. Rev*. **151**, 367 (1966).
12. A. Abragam and B. Bleaney, *Electron Paramagnetic Resonance of Transition Ions*, Oxford: Clarendon (1970).
13. S.E. Barnes, *Adv. Phys*. **30**, 801 (1981).
14. P.E. Tannewald, *Phys. Rev*. **100** (6), 1713 (1955).
15. N.I. Solin, V.V. Ustinov, and S.V. Naumov, *Phys. Solid State* **50** (5), 864 (2008).
16. Ch.P. Poole, *Electron Spin Resonance*, John Wiley & Sons (1967).